

---

This is an electronic reprint of the original article.  
This reprint may differ from the original in pagination and typographic detail.

Turc, L.; Fontaine, D.; Escoubet, C. P.; Kilpua, E.K.J.; Dimmock, A. P.

**Statistical study of the alteration of the magnetic structure of magnetic clouds in the Earth's magnetosheath**

*Published in:*  
Journal of Geophysical Research: Space Physics

*DOI:*  
[10.1002/2016JA023654](https://doi.org/10.1002/2016JA023654)

Published: 01/03/2017

*Document Version*  
Publisher's PDF, also known as Version of record

*Please cite the original version:*  
Turc, L., Fontaine, D., Escoubet, C. P., Kilpua, E. K. J., & Dimmock, A. P. (2017). Statistical study of the alteration of the magnetic structure of magnetic clouds in the Earth's magnetosheath. *Journal of Geophysical Research: Space Physics*, 122(3), 2956-2972. <https://doi.org/10.1002/2016JA023654>

---

This material is protected by copyright and other intellectual property rights, and duplication or sale of all or part of any of the repository collections is not permitted, except that material may be duplicated by you for your research use or educational purposes in electronic or print form. You must obtain permission for any other use. Electronic or print copies may not be offered, whether for sale or otherwise to anyone who is not an authorised user.

## RESEARCH ARTICLE

10.1002/2016JA023654

## Statistical study of the alteration of the magnetic structure of magnetic clouds in the Earth's magnetosheath

## Key Points:

- We study the modification of the magnetic field direction of 82 magnetic clouds (MCs) across the bow shock and in the magnetosheath
- Their magnetic field direction varies significantly across the quasi-parallel shock, and the sign of  $B_z$  can change in the magnetosheath
- Changes in the sign of  $B_z$  are associated with a large  $B_y$ , suggesting that this component may also affect the geoeffectivity of a MC

## Correspondence to:

L. Turc,  
[luclie.turc@esa.int](mailto:luclie.turc@esa.int)

## Citation:

Turc, L., D. Fontaine, C. P. Escoubet, E. K. J. Kilpua, and A. P. Dimmock (2017), Statistical study of the alteration of the magnetic structure of magnetic clouds in the Earth's magnetosheath, *J. Geophys. Res. Space Physics*, 122, 2956–2972, doi:10.1002/2016JA023654.

Received 4 NOV 2016

Accepted 15 FEB 2017

Accepted article online 20 FEB 2017

Published online 7 MAR 2017

L. Turc<sup>1</sup> , D. Fontaine<sup>2</sup> , C. P. Escoubet<sup>1</sup>, E. K. J. Kilpua<sup>3</sup>, and A. P. Dimmock<sup>4</sup> 

<sup>1</sup> Scientific Support Office, Directorate of Science, European Space Research and Technology Centre (ESA/ESTEC), Noordwijk, Netherlands, <sup>2</sup>LPP, CNRS, Ecole polytechnique, UPMC Univ Paris 06, Univ Paris Sud, Observatoire de Paris, Universit Paris-Saclay, Sorbonne Universit, PSL Research University, Ecole Polytechnique, Palaiseau, France, <sup>3</sup>Department of Physics, University of Helsinki, Helsinki, Finland, <sup>4</sup>Department of Radio Science and Engineering, School of Electrical Engineering, Aalto University, Espoo, Finland

**Abstract** The magnetosheath plays a central role in the solar wind-magnetospheric coupling. Yet the effects of its crossing on solar wind structures such as magnetic clouds (MCs) are generally overlooked when assessing their geoeffectivity. Using 82 MCs observed simultaneously in the solar wind and the magnetosheath, we carry out the first statistical study of the alteration of their magnetic structure in the magnetosheath. For each event, the bow shock properties are obtained from a magnetosheath model. The comparison between the model results and observations shows that in 80% of cases, the MHD-based model captures well the magnetosheath transition; the other events are discussed separately. We find that just downstream of the bow shock the variation of the magnetic field direction shows a very good anticorrelation ( $r = -0.91$ ) with the angle between the upstream magnetic field and the shock normal. We then focus on the magnetic field north-south component  $B_z$  because of its importance for geoeffectivity. Although the sign of  $B_z$  is generally preserved in the magnetosheath, we also find evidence of long-lasting intervals of opposite  $B_z$  signs in the solar wind and the magnetosheath during some events, with a  $|B_z|$  reversal  $> 10$  nT at the magnetopause. We find that these reversals are due to the draping of the field lines and are associated with predominant upstream  $B_y$ . In those cases, the estimated position of the regions of antiparallel fields along the magnetopause is independent of the sign of the upstream  $B_z$ . This may have strong implications in terms of reconnection.

## 1. Introduction

The interaction of the supersonic solar wind with the Earth's magnetosphere creates a bow shock through which the incoming flow is decelerated to subsonic speeds. The magnetosheath is the region occupied by the shocked solar wind plasma, heated, and compressed, extending from the bow shock to the magnetopause. Because it is actually the magnetosheath plasma which comes in contact with the magnetopause, its properties are crucial for the energy, plasma, and momentum transfer from the solar wind to the magnetosphere [e.g., Lopez *et al.*, 2010; Pulkkinen *et al.*, 2016]. The magnetosheath is a highly variable region, since its spatial and temporal plasma properties respond to the upstream solar wind state but also because of the self-generated turbulence and instabilities which arise locally. The spatial variation mostly stems from the varying bow shock parameters encountered upon entering the magnetosheath and especially the angle  $\Theta_{Bn}$  between the local shock normal and the upstream magnetic field vector. The contrast between the quasi-perpendicular ( $\Theta_{Bn} > 45^\circ$ ) and quasi-parallel ( $\Theta_{Bn} < 45^\circ$ ) regimes gives rise to pronounced asymmetries in the magnetosheath because the processing of the plasma through the bow shock varies as a function of  $\Theta_{Bn}$  [Walsh *et al.*, 2012; Dimmock and Nykyri, 2013; Walsh *et al.*, 2014; Dimmock *et al.*, 2015, 2016, and references therein]. For example, because only the tangential component of the magnetic field increases through the bow shock, the magnetosheath magnetic field is stronger downstream of the quasi-perpendicular bow shock. The magnetic field lines are also distorted as they drape around the magnetosphere. Furthermore, when the magnetosheath plasma  $\beta$  is low, accelerated flows can be observed along the magnetopause flanks [e.g., Rosenqvist *et al.*, 2007; Lavraud and Borovsky, 2008; Erkaev *et al.*, 2012; Lavraud *et al.*, 2013, and references therein]. This is due to the fact that in such conditions, the magnetic forces become predominant inside the magnetosheath. The upstream conditions for magnetopause processes, such as magnetic reconnection [Dungey, 1961] and the Kelvin-Helmholtz instability (KHI) [Hasegawa *et al.*, 2004], are dictated by the local magnetosheath properties.

Their spatial variations can therefore influence where magnetopause processes occur, for example, favoring one flank for the KHI [Taylor et al., 2012; Nykyri, 2013]. This is attributed to the lower tangential magnetic field in the quasi-parallel magnetosheath, which would increase the growth rate of the KHI.

The influence of the bow shock crossing and the subsequent convection in the magnetosheath on large-scale solar wind transients is generally overlooked. In particular, it is generally assumed that the magnetic field direction, which is central for reconnection, remains unchanged downstream of the bow shock. Consequently, the geoeffectivity of the structure is estimated based on its properties in the solar wind only. However, a number of studies convey convincing evidence that the magnetic field direction can change significantly from the solar wind to the magnetosheath, thus questioning the validity of this assumption. For example, Coleman [2005] focuses on the magnetic field clock angle, measured in the plane perpendicular to the Sun-Earth line and compares observations in the solar wind and along the magnetopause. The results show that 30% of the time, this angle varies by more than  $30^\circ$  from the solar wind to the magnetosheath. The author concludes that the “perfect draping approximation,” i.e., which the clock angle is preserved in the magnetosheath, is not accurate enough to estimate the magnetic field direction along the magnetopause. In Longmore et al. [2006], spacecraft observations in the magnetosheath are compared to the predictions of the Kobel and Flückiger [1994] field line draping model. A rotation of the clock angle ranging from  $5$  to  $30^\circ$  is found, which is attributed to field-flow coupling effects not taken into account in the Kobel and Flückiger [1994] model. We stress here that a variation of the clock angle can result in a change of the sign of the magnetic field north-south ( $B_z$ ) component. The sign of  $B_z$  is fundamental for geoeffectivity because a southward  $B_z$  upstream of the magnetopause is conducive to reconnection with the Earth’s magnetic field in the subsolar region. The probability of observing different  $B_z$  signs upstream and downstream of the bow shock is investigated in Šafránková et al. [2009]. They find that the probability of the correct prediction of the sign of the magnetosheath  $B_z$  based on that in the solar wind is close to random coincidence for low  $|B_z|$  values, and increases with  $|B_z|$ . Yet it does not always reach 1 even for the highest  $|B_z|$ . An example of such a change of the  $B_z$  sign for a predominantly southward interplanetary magnetic field (IMF) is presented in Němeček et al. [2015].

In this study, we focus on a specific type of large-scale solar wind transients called magnetic clouds (MCs). MCs are a subset of coronal mass ejections which possess a well-defined magnetic structure in the interplanetary space. They are characterized by an enhanced and smoothly rotating magnetic field, generally accompanied by a depressed proton temperature [Burlaga et al., 1981]. MCs are the drivers of the most intense geomagnetic storms [Huttunen et al., 2005; Echer et al., 2008; Yermolaev et al., 2012]. Understanding how they interact with the Earth’s environment is thus crucial for space weather forecasting. Many studies [e.g., Gopalswamy et al., 2008; Ji et al., 2010; Hidalgo et al., 2011, and references therein] focus on establishing linear correlations between one or a combination of the MC’s parameters with the level of geomagnetic activity as estimated from ground-based indices, in order to predict the geoeffectivity of upcoming events. Yet the correlation coefficients obtained in these kind of studies rarely reach 0.9 [Gopalswamy et al., 2008] but are generally lower [e.g., Borovsky, 2013]. Moreover, a very large scatter of the parameters is observed for the most extreme values. The linear correlation thus tends to decline for the strongest events. Therefore, a closer scrutiny of the processes at play when MCs interact with the Earth’s environment is needed.

The first steps of this interaction are the crossing of the terrestrial bow shock and the propagation into the magnetosheath. The MCs’ properties, and in particular their magnetic field direction, are expected to be significantly altered through these regions, as is the case for the regular solar wind. Furthermore, we note that MCs are characterized by a low Alfvén Mach number ( $M_A$ ), generally below 5 [Lavraud and Borovsky, 2008; Turc et al., 2016]. These low  $M_A$  conditions in the solar wind alter the volume of the magnetosheath, which becomes much larger than usual as the bow shock moves outward, but also how energy is processed at the bow shock [e.g., Treumann, 2009], the magnetosheath flows [Lavraud et al., 2007; Farrugia et al., 2013], the current systems in the Earth’s environment [Lopez et al., 2011], and more generally, the solar wind-magnetospheric coupling during MC events [Lopez et al., 2004; Lavraud and Borovsky, 2008; Farrugia et al., 2013; Myllys et al., 2016]. Because MCs correspond to atypical conditions, it is particularly interesting to investigate how they evolve across the bow shock and into the magnetosheath. Eastwood et al. [2002] used combined spacecraft observations in the solar wind and the magnetosheath to study the evolution of a small-scale flux rope across the bow shock. They showed that the bow shock crossing causes a rotation of the flux rope axis. More recently, a few case studies of MCs observed simultaneously in the solar wind and the magnetosheath were presented

in *Turc et al.* [2014a]. The results, supported by modeling and numerical simulations [*Turc et al.*, 2014b, 2015], suggest that the modification of the magnetic field direction across the bow shock is directly controlled by the angle  $\Theta_{Bn}$ .

The aim of the present paper is to extend the results of the *Turc et al.* [2014a] case studies through a comprehensive statistical study. In particular, we will examine the relationship between  $\Theta_{Bn}$  and the variation of the magnetic field direction, and attempt to establish an empirical relationship linking these two parameters. We will also investigate how this variation is distributed on the different magnetic field components and especially how  $B_z$  is affected. We will focus on the cases when  $B_z$  has a different sign upstream and downstream of the bow shock and look for conditions when this take place. Finally, this statistical study will also allow us to test the performances of the magnetosheath model introduced in *Turc et al.* [2014b] on a large number of events. The paper is structured as follows: in section 2, we describe the data sets, the magnetosheath model, and the methodology used in the study. In section 3 the main results of this work are presented. Section 4 analyzes the events which were not correctly modeled and discusses the limitations of the magnetosheath model. Finally, section 5 provides a summary and a discussion of our main findings.

## 2. Data Set and Methodology

This study is based on the MC catalog introduced in *Turc et al.* [2016], which lists the MCs observed near the Sun-Earth  $L_1$  libration point from 2000 to 2014. For each of these MCs, our list also indicates in which region (i.e., solar wind, magnetosheath or magnetosphere) the following spacecraft can be found: Cluster [*Escoubet et al.*, 2001], the Time History of Events and Macroscale Interactions during Substorms (THEMIS) [*Angelopoulos*, 2008], the Geomagnetic Tail Lab (GEOTAIL) [*Nishida*, 1994], Interball-Tail [*Galeev et al.*, 1996], and Double-Star TC1 [*Liu et al.*, 2005]. Note that the identification of the different geophysical regions is not based on models of their boundaries but on the inspection of the actual spacecraft data for each MC. This facilitates the selection process for all kind of studies focusing on the interaction of MCs and of their sheath regions with the near-Earth space.

Here we select the MCs during which spacecraft observations are available in the dayside magnetosheath, with at least 1 h of continuous sampling of this region. We find 82 suitable MCs, out of which 32 (39%) even have two spacecraft or more in the dayside magnetosheath during the same MC, though not necessarily simultaneously. This yields a total of 129 sets of magnetosheath measurements during a MC (hereafter referred to as "events"), when taking into account separately the contribution of the different spacecraft. Note that the Cluster fleet is considered as a single spacecraft as the spacecraft separations are much smaller than the scales of interest. Likewise, the different THEMIS satellites are only included if the interspacecraft separation exceeds  $2 R_E$ . This study is drawn upon magnetic field measurements from the fluxgate magnetometers aboard Cluster [*Balogh et al.*, 1997], THEMIS [*Auster et al.*, 2008], and Double-Star [*Carr et al.*, 2005]; the magnetic field experiment [*Kokubun et al.*, 1994] aboard GEOTAIL and from the FM-3I; and the multicomponent investigations of fluctuations magnetometers [*Nozdrachev et al.*, 1995; *Klimov et al.*, 1997] aboard Interball-Tail. Note that all vector quantities will be given in the Geocentric Solar Ecliptic (GSE) coordinate system throughout this paper.

As demonstrated in previous studies [e.g., *Turc et al.*, 2014a], the modification of the properties of MCs from the solar wind to the magnetosheath is strongly controlled by the bow shock configuration. To interpret the observations, it is therefore necessary to know the local value of  $\Theta_{Bn}$  associated with each of our magnetosheath samples. Since we cannot directly measure this angle, we use a magnetosheath model [*Turc et al.*, 2014b] to estimate where the streamline passing through the spacecraft in the magnetosheath intersects the bow shock and what is the corresponding  $\Theta_{Bn}$  value. The inputs of the model are the solar wind parameters, which are primarily taken from the magnetic field experiment (MAG) [*Smith et al.*, 1998] and the Solar Wind Proton, Electron and Alpha Monitor [*McComas et al.*, 1998] aboard the Advanced Composition Explorer (ACE) [*Stone et al.*, 1998] spacecraft. Alternatively, the OMNI data set propagated to the Earth's bow shock, or the Magnetic Field Investigation [*Lepping et al.*, 1995], and the Solar Wind Experiment [*Ogilvie et al.*, 1995] measurements from the Wind spacecraft [*Acuña et al.*, 1995] are used when there are large gaps in ACE data. Each event is divided into 5 min intervals, over which the data are averaged, as was done in *Turc et al.* [2016]. This is necessary because the magnetosheath model requires quasi-steady upstream parameters as inputs in order to ensure that the flow pattern in the magnetosheath remains nearly steady while the plasma propagates from the bow shock to the spacecraft. Averaging the data also reduces the errors due to the time shift of the

solar wind measurements from  $L_1$  to Earth. On the other hand, it is also important not to degrade excessively the resolution of the data because the bow shock and the magnetosheath properties would respond rather quickly, i.e., in a matter of minutes, to changes in the upstream state and our samples need to be representative of the simultaneous upstream and downstream conditions. The 5 min windows were therefore selected as a trade-off between a good time resolution and the requirements of the magnetosheath model.

In order to perform this statistical study, some modifications were made in the magnetosheath model in order to optimize its results. First, the compression ratio is now calculated using the formula established by *Borovsky* [2013], which provided a better agreement between model and observations than the formula of *Landau and Lifshitz* [1959]. Second, the bow shock model of *Jeřáb et al.* [2005] employed in the initial version of the model was chosen because of its better performance in the low- $M_A$  range [*Turc et al.*, 2013], but not all MCs are associated with low- $M_A$  conditions. We have thus implemented a second bow shock model [*Měrka et al.*, 2005] into the magnetosheath model in order to better describe the events with higher  $M_A$ . On these events, the magnetosheath model was run with each of the bow shock models and we selected whichever model provided the best estimates of the observed magnetosheath magnetic field. When  $M_A > 5$ , the *Měrka et al.* [2005] generally gave better results than the *Jeřáb et al.* [2005] model.

To validate the results of the magnetosheath model, we compare its prediction of the magnetic field direction at the spacecraft position with the actual measurements. A first selection was done by visual inspection: if the model visibly failed to globally predict the magnetic field orientation and its overall temporal variations, the event was discarded (criterion 1). Among the retained events, we then calculated the angle between modeled and observed magnetosheath magnetic fields and selected only those 5 min samples for which the model correctly estimates the magnetic field direction in the magnetosheath within  $10^\circ$  (criterion 2). The model satisfactorily reproduces the observations for 103/129 events (80%) (selected with criterion 1), which yield a total of  $> 5900$  samples satisfying criterion 2. Note that our selection method allows for isolated samples to be selected, for which criterion 2 may in some cases be satisfied accidentally. We estimate that our data set contains 3% of isolated samples, which should not affect the results of our analysis. The events we completely discarded will be further examined in the discussion. To each magnetosheath sample are associated a number of parameters determined from the magnetosheath model, in particular the angle  $\Theta_{Bn}$  encountered upon entering the magnetosheath and the fractional distance inside the magnetosheath:

$$F = (r - r_{mp}) / (r_{bs} - r_{mp}) \quad (1)$$

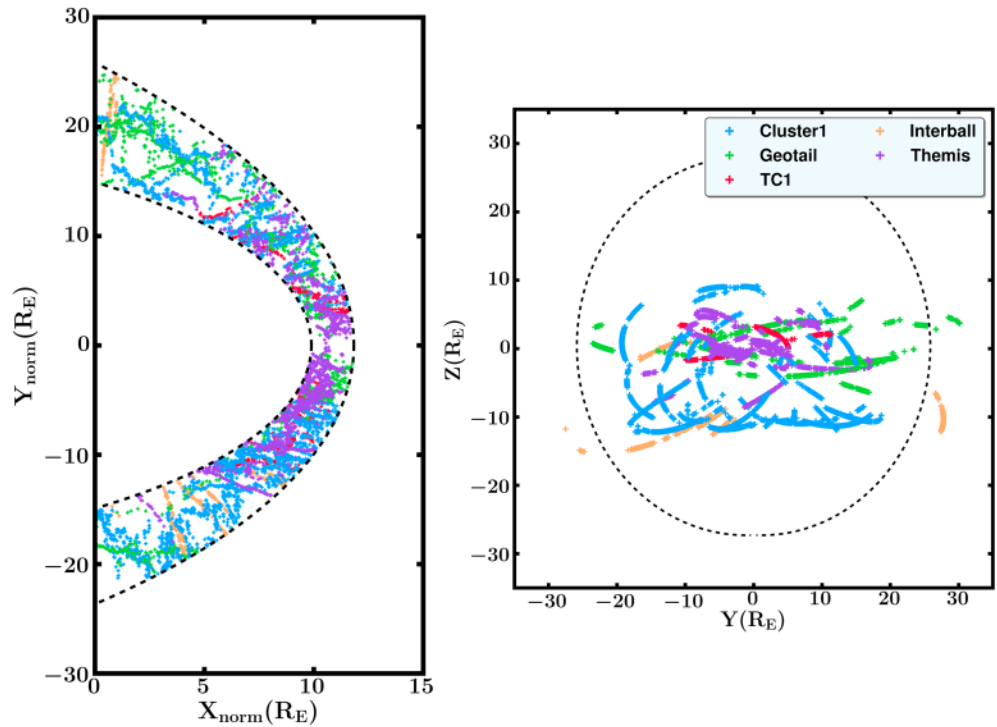
[*Soucek and Escoubet*, 2012, and references therein], where  $r$ ,  $r_{bs}$ , and  $r_{mp}$  are the geocentric distances of the spacecraft, the bow shock, and the magnetopause, respectively (along the Earth-spacecraft direction).

Figure 1 displays the position of the magnetosheath samples, color coded according to the spacecraft from which the measurements were taken. In Figure 1 (left), the position of the data points is normalized in order to illustrate their distribution relative to the magnetosheath boundaries. The average bow shock and magnetopause positions (dashed black lines) were obtained from the *Jeřáb et al.* [2005] and *Shue et al.* [1998] models, respectively, with the average MC parameters as the input ( $n = 6.5 \text{ cm}^{-3}$ ,  $V = 482 \text{ km s}^{-1}$ ,  $B = 12.4 \text{ nT}$ ,  $B_z = 0$ ; see *Turc et al.* [2016]). Each data point is then plotted inside this “average magnetosheath,” its position being determined by its solar zenith angle and its fractional distance  $F$  between the magnetosheath boundaries as determined with the magnetosheath model. Figure 1 (right) shows the position of our samples in the GSE YZ plane, where the dashed black line corresponds to the bow shock position in the terminator plane. Our data set is mostly concentrated near the equatorial plane because of the orbits of the spacecraft sampling the magnetosheath. Only Cluster (blue) and Interball-Tail (brown) probe the higher latitudes, thus providing some data points beyond  $|Z| = 10 R_E$ . However, as shown in Figure 1 (left), we have a very good coverage of the relative distances between the bow shock and the magnetopause, and of the angular distance from the Sun-Earth line, except very close to the subsolar point. Our data set thus covers most of the low-latitude dayside magnetosheath.

### 3. Results

#### 3.1. Magnetic Field Direction

We first investigate the variation of the magnetic field direction across the bow shock. In order to quantify its modification, we define  $\psi$  as the angle between the magnetic field vector in the solar wind and that in the magnetosheath. Figure 2 shows a scatter plot of this angle  $\psi$  as a function of the  $\Theta_{Bn}$  value encountered at



**Figure 1.** (left) Position of the magnetosheath samples relative to the magnetosheath boundaries (see text for more detail) and (right) in the GSE YZ plane. The colors indicate from which spacecraft the data were obtained (Cluster: blue; Interball-Tail: orange; GEOTAIL: green; Double-Star-TC1: red; THEMIS: purple). The dashed lines correspond to modeled bow shock and magnetopause (Figure 1, left, only) for average MC conditions, in the equatorial plane (Figure 1, left), and in the terminator plane (Figure 1, right).

the bow shock, estimated from the magnetosheath model, for each of the 5 min magnetosheath samples. There is a clear tendency for  $\psi$  to increase as the shock configuration becomes more parallel. The color scale indicates the fractional distance inside the magnetosheath (as defined in equation 1). The light blue points correspond to observations near the magnetopause, while the magenta points are located just downstream of the bow shock. We find that the observations near the bow shock are clustered in a rather narrow range, while most of the scatter is due to the measurements in the vicinity of the magnetopause.

The solid black line shows a linear fit of the entire data set, with the equation of the best fit line being the following:  $\psi = 64.8^\circ - 0.659\Theta_{Bn}$ , associated with a fairly good anticorrelation ( $r = -0.76$ ). If we restrict to the data points in the first 30% of the magnetosheath from the bow shock inward, i.e., at a fractional distance  $F > 0.7$ , the correlation coefficient increases to 0.91. The equation of the line is then

$$\psi = 60.3^\circ - 0.647\Theta_{Bn} \tag{2}$$

The slope of the line does not vary significantly, but it comes closer to  $\psi = 0^\circ$  for  $\Theta_{Bn} = 90^\circ$  with the reduced data set, which is what we would expect from Rankine-Hugoniot equations. The goodness of both linear fits is also illustrated by the very narrow 99% confidence intervals (green lines). The larger scatter of the samples for the entire data set most likely stems from the fact that other processes such as field line draping come into play when moving deeper into the magnetosheath. Also, wave activity increases closer to the magnetopause, which can augment the spread of the data.

We now compare our data with MHD predictions, in order to illustrate the expected behavior of  $\psi$  as a function of  $\Theta_{Bn}$  just downstream of the bow shock. Since the solar wind parameters are relatively steady during MCs, and we consider 5 min averaged data both upstream and downstream of the shock; Rankine-Hugoniot relations can be applied to our data sets to describe the bow shock crossing. From the equations of Rankine-Hugoniot and assuming that magnetic coplanarity is satisfied and that the tangential velocity is

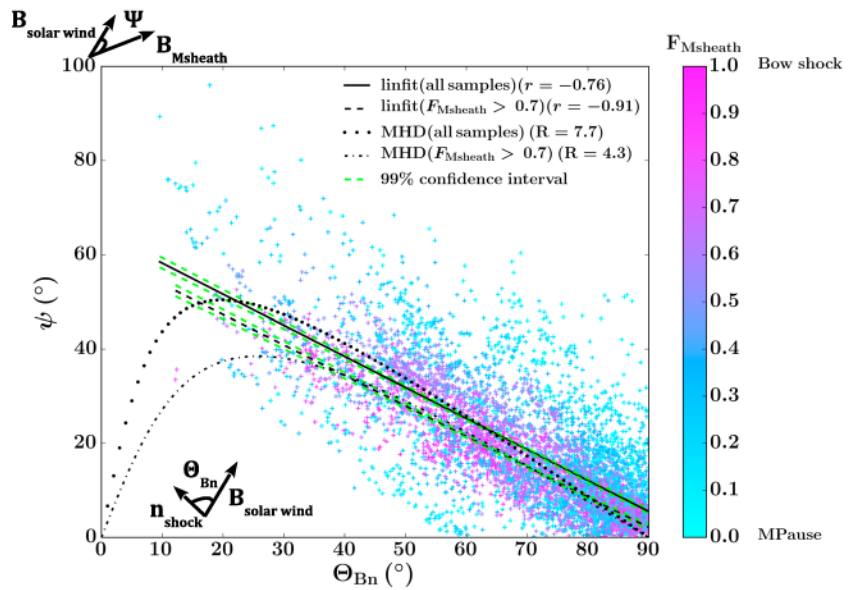


**Figure 2.** Scatter plot:  $\Theta_{Bn}$  as a function of the angle  $\psi$  between the magnetic field vectors in the solar wind and the magnetosheath, color coded as a function of the fractional distance inside the magnetosheath. Both angles are schematized on the figure. Black curves: linear fit of the entire data set (solid line), of the reduced data set ( $F > 0.7$ ; dashed line), fit based on MHD equations (see text) of the entire data set (dotted line) and of the reduced data set (dash-dotted line). The green lines show the 99% confidence intervals for both linear fits.

conserved across the bow shock (see *Génot et al.* [2011] for a discussion of this last assumption), the relationship between  $\Theta_{Bn}$  and  $\psi$  can be written as

$$\psi = \arctan(R \tan(\Theta_{Bn})) - \Theta_{Bn} \tag{3}$$

where  $R$  is the bow shock compression ratio, i.e., the ratio of downstream to upstream density. At the Earth’s bow shock, this parameter usually ranges between 3 and 4 and varies as a function of the upstream conditions, in particular the magnetosonic Mach number. According to MHD theory [*Farris and Russell*, 1994; *Borovsky*, 2013],  $R$  tends toward 4 when the Mach number tends to infinity (assuming that the ratio of specific heats  $\gamma = 5/3$  in the formula of *Farris and Russell* [1994]). The only free parameter being the compression ratio, we perform a least squares fitting of the entire data set (dotted line in Figure 2) and of the reduced data set ( $F > 0.7$ ; dash-dotted line). Because the magnetosheath model employed to calculate  $\Theta_{Bn}$  is based on the assumptions listed above, equation (3) should be verified in the outer parts of the magnetosheath, i.e., just behind the shock. However Rankine-Hugoniot relations may not be obeyed for some cases as they are not valid inside the shock transition nor when the shock is not stationary. The values obtained for the compression ratio both exceed the upper limit given by the MHD. We interpret this as the consequence of the pileup of the field lines in front of the magnetopause. We checked that if only the samples very close to the bow shock ( $F > 0.9$ ) are considered, we obtain  $R = 3.6$ , which is consistent with the MHD predictions. As illustrated by the dotted line being above the dash-dotted line in Figure 2, a larger compression results in a larger  $\psi$  for a given  $\Theta_{Bn}$ . Since the compression ratios obtained from the fits are above 4, this means that overall the propagation in the magnetosheath further increases  $\psi$ .

Interestingly, for  $\Theta_{Bn} \leq 25^\circ$ , the MHD description predicts a decrease of  $\psi$  when  $\Theta_{Bn}$  tends toward zero. However, no conclusive evidence of this decrease can be found in our data set because of the scarcity of our samples for the lowest  $\Theta_{Bn}$  values and their scatter. Two factors contribute to the poor coverage of the lowest  $\Theta_{Bn}$  values ( $\Theta_{Bn} < 30^\circ$ , hereafter termed “strongly parallel”). First, this configuration is less frequently observed than the quasi-perpendicular geometry on the dayside bow shock during MCs [*Turc et al.*, 2016]. Second, we only retained here the samples for which we had a good agreement between model and observations. Yet the MHD description used in the model is not sufficient to capture all the features of the quasi-parallel shock configuration, where kinetic processes dominate. Hence, the complete absence of data points below  $\Theta_{Bn} = 10^\circ$

and the sparse observations below  $30^\circ$ . Moreover, equation (3) is only valid just downstream of the bow shock, which may also explain why we do not observe the decrease of  $\psi$  at low  $\Theta_{Bn}$ . It is therefore difficult to draw any firm conclusion for the strongly parallel regime.

At higher  $\Theta_{Bn}$  values, the functions derived from MHD are approximately linear. We use the sum of the squared residuals to compare the quality of the different fittings. We find that the fit quality is relatively insensitive to employing either the linear fitting or the function derived from MHD, but that using the data set restricted to  $F > 0.7$  significantly improves it. Therefore, we conclude that equations (2) and (3), despite the assumptions required to apply the latter, both provide a simple and fairly reliable way of estimating  $\psi$  in the outer magnetosheath. Deeper in the magnetosheath, as data becomes more scattered, the fit quality is lower but remains acceptable. Overall, we find that for  $\Theta_{Bn} > 30^\circ$ ,  $\psi$  increases linearly as  $\Theta_{Bn}$  decreases.

However,  $\psi$  only gives us information about the overall variation of the magnetic field orientation but not which components will be affected by those changes. We now investigate how the magnetic field cone angle  $\theta_{Bx} = \cos^{-1}(B_x/B)$  and clock angle  $\phi_c = \cos^{-1}(B_z/\sqrt{B_y^2 + B_z^2})$  are modified from the solar wind (sw) to the magnetosheath (Msheath). Figure 3a displays the variation of the cone angle  $\Delta\theta_{Bx} = \theta_{Bx}^{\text{Msheath}} - \theta_{Bx}^{\text{sw}}$  as a function of the  $\psi$  angle. The data points are visibly clustered around  $\Delta\theta_{Bx} = \pm\psi$ , thus revealing that most of the variation of the magnetic field direction translates into a change of the cone angle. The positive  $\Delta\theta_{Bx}$  are associated with  $\theta_{Bx}^{\text{sw}} < 90^\circ$ , while negative values are obtained when  $\theta_{Bx}^{\text{sw}} > 90^\circ$ . This shows that the field lines tend to rotate away from the Sun-Earth line, consistent with their draping around the dayside magnetopause. As expected from Figure 3a, Figure 3b shows that  $\Delta\phi_c$  is much smaller than  $\Delta\theta_{Bx}$  and remains generally below  $20^\circ$ .

We propose the following interpretation for the distribution of the variation on  $\theta_{Bx}$  and  $\phi_c$ . At the bow shock nose, the normal direction is aligned with the Sun-Earth line. We have thus  $B_x = B_n$ , and the GSE YZ plane corresponds to the bow shock tangential plane. This configuration is illustrated schematically in the lower left part (1) of Figure 3d, where the dark purple surface is the bow shock. The tangential vectors  $t_1$  and  $t_2$  are contained in the GSE YZ plane, materialized by the lilac rectangle. (u) denotes the values upstream, and (d) the values downstream of the bow shock. Because of magnetic coplanarity, which is assumed to hold here, the tangential components (here  $B_y$  and  $B_z$ ) have the same direction across the shock [Treumann, 2009], as shown in Figure 3d by the vectors  $B_t(u)$  (yellow) and  $B_t(d)$  (green). Therefore,  $\phi_c$  is preserved at the crossing of the subsolar bow shock, while  $\theta_{Bx}$  varies as the IMF is rotated away from the shock normal. When moving toward the dawn-dusk terminator (at any latitude), the plane tangential to the shock's surface departs progressively from the GSE YZ plane. This is illustrated in the upper right part (2) of Figure 3d, where the shock tangential plane, shown by the dark blue rectangle, is no longer parallel to the GSE YZ plane. The variation of  $\phi_c$  should therefore increase with increasing distance from the subsolar point. This is confirmed by Figure 3c, which shows the variation of  $\phi_c$  just downstream of the bow shock. Each sample is color coded according to the solar zenith angle. In the subsolar region (dark blue points),  $\phi_c$  remains roughly unchanged at the bow shock's crossing, while further on the flanks (green points) its variation can reach up to  $40^\circ$ . The propagation inside the magnetosheath causes a further variation of  $\phi_c$ , independently of the solar zenith angle but which remains relatively modest, below  $10^\circ$  in 85% of the cases (not shown). On the contrary, the draping of the field lines affects  $\theta_{Bx}$  more prominently so that the field lines progressively become tangential to the magnetopause. The combination of these different mechanisms causes the large variation of  $\theta_{Bx}$ , while  $\phi_c$  shows only minor deviations.

In terms of the magnetic field components, this implies that near the equatorial plane, the traversal of the magnetosheath will mostly change the relative importance and possibly the signs of  $B_x$  and  $B_y$ , while in the noon-midnight meridian plane, it will essentially affect  $B_x$  and  $B_z$ . Note that the magnitude of all components will also be modified due to the magnetic compression at the bow shock's crossing and the piling up of the field lines at the magnetopause.

### 3.2. $B_z$ Component

We now concentrate on the  $B_z$  component of the magnetic field because of its pivotal role for geoeffectivity. In Figure 4a we have plotted the  $B_z$  component measured inside the magnetosheath as a function of that in the upstream solar wind. Each data point is color coded according to the fractional distance inside the magnetosheath. Contrary to the  $\psi$  angle whose values are more scattered deeper into the magnetosheath (see section 3.1), the spread of the magnetosheath  $B_z$  does not increase when approaching the magnetopause.

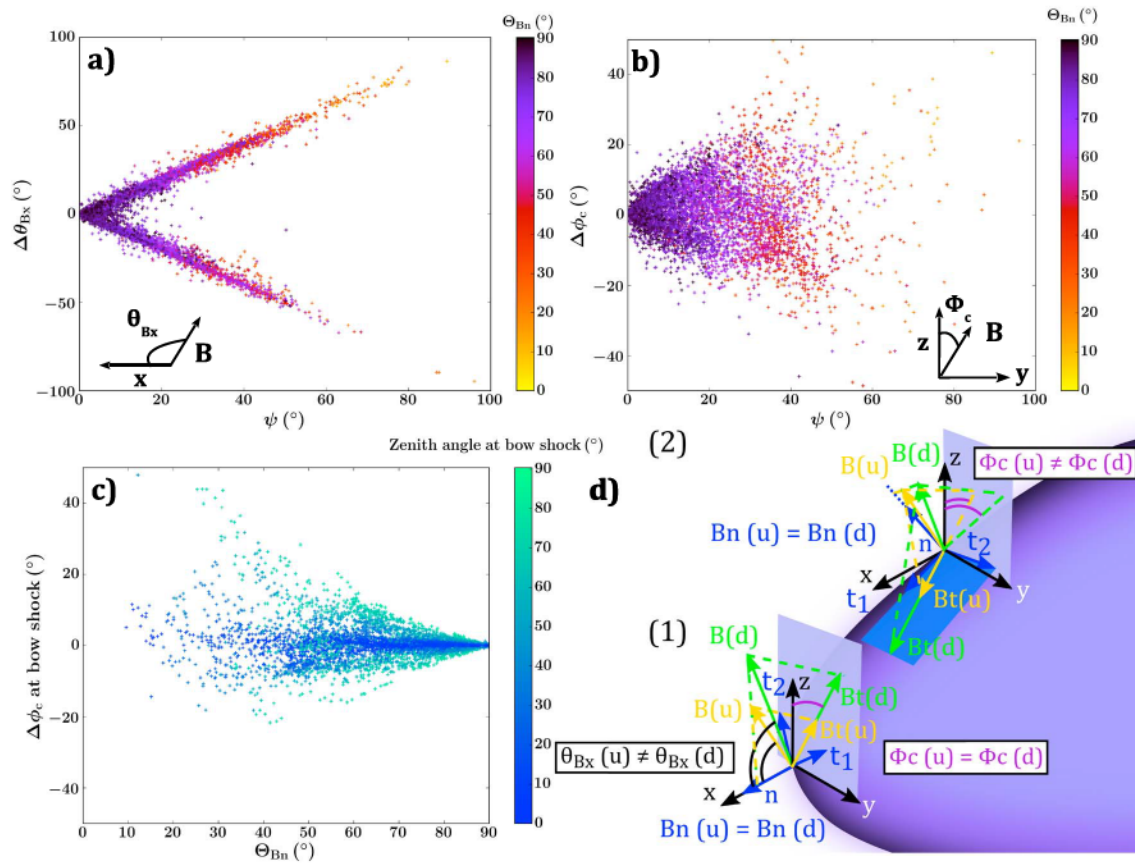


**Figure 3.** Scatter plots of the variation of (a) the cone angle and (b) the clock angle from the solar wind to the magnetosheath, as a function of  $\psi$ . The color code indicates the  $\Theta_{Bn}$  associated with each of the samples. (c) Variation of the clock angle from the solar wind to the immediate downstream of the bow shock, as a function of  $\Theta_{Bn}$ . The color code shows the zenith angle, measured from the Sun-Earth line. (d) Schematic of the modification of the magnetic field direction across the bow shock (dark purple surface) at the bow shock nose (1) and farther on the flanks (2). (u) Denotes the upstream vectors (yellow) and (d) the downstream vectors (green). The reference frames in black are aligned with the GSE frame, while the reference frames in blue are the local frames defined by the shock normal direction ( $n$ ) and the plane tangential to the shock surface ( $t_1$  and  $t_2$ ).  $B_t$  refers to the projection of the magnetic field in the tangential plane while  $B_n$  is the magnetic field normal component, which is preserved across the bow shock. The magnetic field cone angles  $\theta_{Bx}$  are indicated by black curves in (1). The magnetic field clock angles  $\phi_c$  are indicated by purple curves.

The distribution of the points in Figure 4 suggests that there is a linear relation between  $B_z$  in the solar wind and in the magnetosheath, which is particularly prominent for  $|B_z^{SW}| < 15$  nT. At larger  $|B_z|$ , the lack of data points and their scattering make it difficult to assess whether this linear relationship persists. The equation of the best fit line obtained from the linear least-squares regression of the whole data set is:  $B_z^{msheath} = 3.19 \times B_z^{SW} - 0.07$ , associated with an excellent correlation coefficient ( $r = 0.95$ ) and a narrow 99% confidence interval (green lines). For the subset of the data points in the vicinity of the bow shock ( $F > 0.7$ ), the correlation coefficient is 0.97. We only find a slightly lower value for the slope (2.87) when  $F > 0.7$ , while its value increases to 3.35 if we restrict to the points where  $F < 0.3$ . In other words,  $B_z$  is about three times stronger in the magnetosheath than in the solar wind, and it only marginally increases when nearing the magnetopause.

Figure 4b presents a close-up of the central part of Figure 4a, with a different color code: red indicates that the sign of  $B_z$  is the same in the solar wind and the magnetosheath, while the samples drawn in blue have opposite  $B_z$  signs. We find that in a number of cases, a southward  $B_z$  can turn north in the magnetosheath, and vice versa. However, the change of the  $B_z$  sign is only significant if its sign can be reliably determined both in the solar wind and the magnetosheath. For a given sample, which corresponds to 5 min averaged measurements, we consider that  $B_z$  is significantly positive (negative) if  $B_z - \sigma(B_z + \sigma)$  is also positive (negative).  $\sigma$  is the standard deviation of  $B_z$  during the considered 5 min interval. This criterion is applied to  $B_z$  in the solar wind and in the magnetosheath. Those samples for which the sign of  $B_z$  is reliable and which have different  $B_z$  signs in the solar wind and the magnetosheath are indicated by the large blue crosses in Figure 4b. Hereafter, the term “ $B_z$  reversals” will refer to the intervals or samples for which the sign of  $B_z$  in the magnetosheath

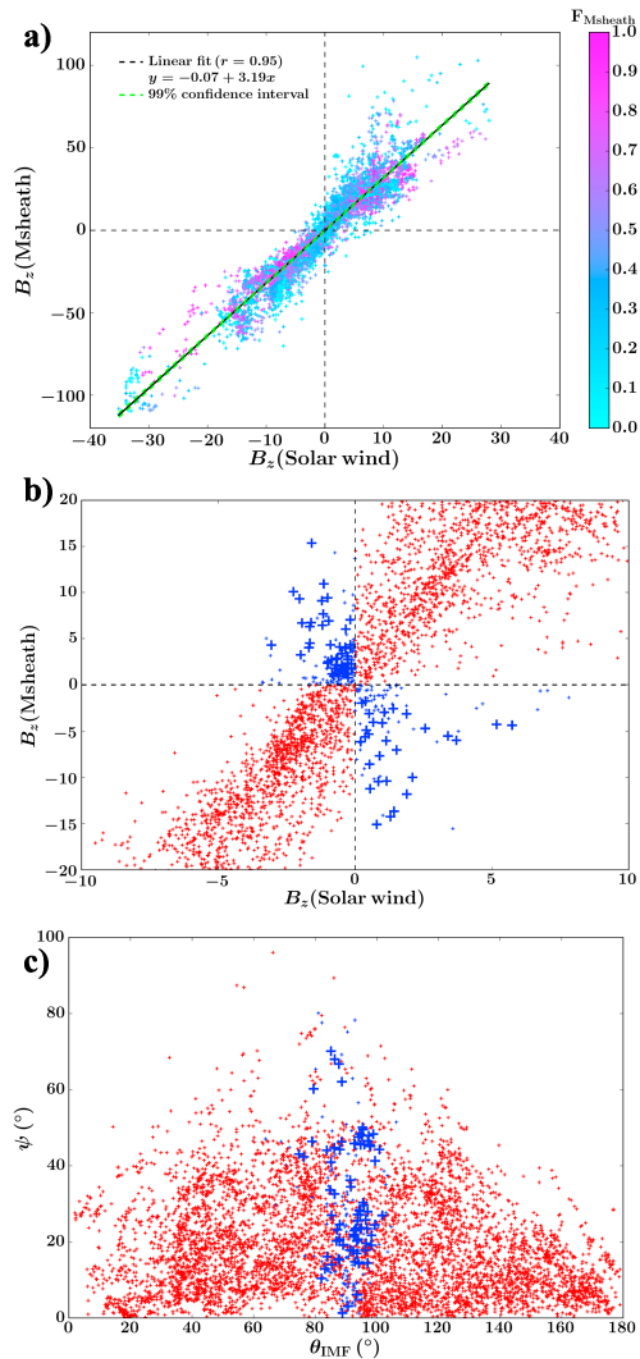


**Figure 4.** (a) Magnetic field  $B_z$  component in the magnetosheath plotted against that in the solar wind. Each data point is colored according to its fractional distance inside the magnetosheath. The black dashed line shows the linear fit of the data set and the green lines the 99% confidence interval. Note that the green lines are overlapping the black line in the central part of the plot. (b) Magnified section of the central part of Figure 4a, with a different color code. The sign of  $B_z$  is the same in the solar wind and the magnetosheath for the red samples, and changes for the blue samples. (c) Scatter plot of the angle  $\psi$  as a function of the angle between the upstream magnetic field vector and the Z axis. Same color code as Figure 4b.

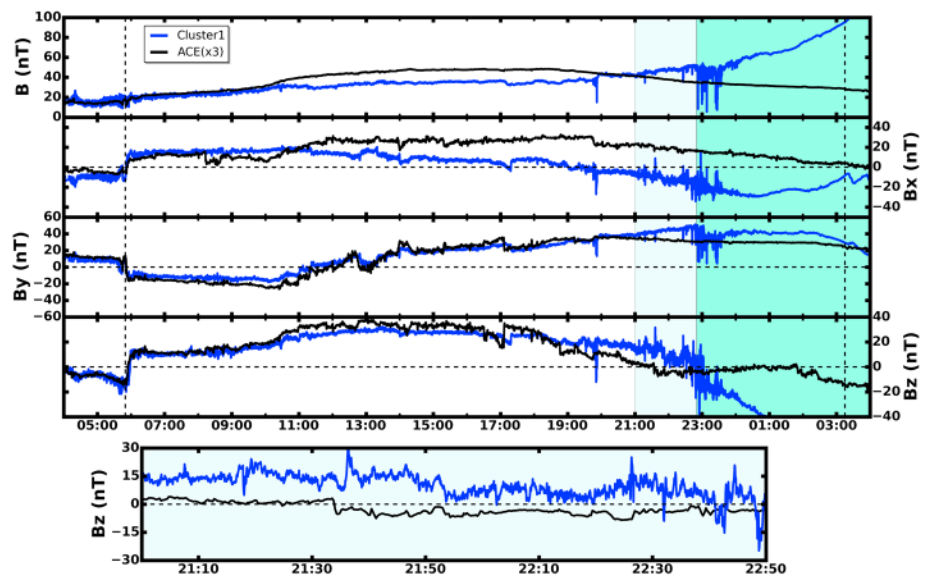


**Figure 5.** ACE (time shifted) (black) and Cluster (blue) observations during the MC starting on 29 November 2006. The vertical lines indicate the leading and trailing edges of the MC. The area highlighted in green shows when Cluster is inside the magnetosphere. From top to bottom: magnetic field strength,  $B_x$ ,  $B_y$ ,  $B_z$ , and magnified section of  $B_z$  in the interval highlighted in grey.

differs from that in the solar wind. Such reversals are observed in 1.4% of our magnetosheath samples. The occurrence rate of the  $B_z$  reversals will be further discussed in section 5. Although most of these data points are rather isolated (4 or less per MC), we also find three events with half an hour or more of uninterrupted observations of a reversed  $B_z$ . Therefore, the sign of the  $B_z$  component of the magnetic field in a region of the magnetosheath can differ from that in the solar wind during extended intervals.

We then investigate in which conditions these  $B_z$  reversals occur. We find no clear ordering of our samples with the shock configuration or the position inside the magnetosheath (not shown), though these parameters were central for the overall variation of the magnetic field direction (see section 3.1). The reversals do not tend to be associated with higher- or lower-latitude spacecraft observations. No relationship with the upstream solar wind parameters can be established either, except with the upstream magnetic field orientation. This is illustrated by Figure 4c, which shows  $\psi$  plotted against the angle  $\theta_{sw} = \arccos(B_z/B)$  in the solar wind. The color code is the same as in Figure 4b, with the data points in blue having different  $B_z$  signs in the solar wind and in the magnetosheath and the large blue crosses indicating the significant  $B_z$  reversals. We note that all blue samples are clustered near  $\theta_{sw} = 90^\circ (\pm 10^\circ)$ , which corresponds to a magnetic field lying close to the equatorial plane, where  $B_z = 0$ . Therefore, we observe a change of the  $B_z$  sign when a limited rotation of the upstream magnetic field direction is sufficient to move from one side of the equatorial plane to the other. The reversal of the  $B_z$  component is, however, independent of the total change of the magnetic field direction across the bow shock, as evidenced by the distribution of the blue data points across all the  $\psi$  values.

As an example, Cluster and ACE magnetic field observations from 04:00 UT on 29 November 2006 to 04:00 UT the next day are shown in Figure 5. This interval encompasses a MC, whose front and rear boundaries are marked by vertical dashed lines. ACE data are lagged by 58 min to account for the offset of ACE being in  $L_1$ . Cluster is located in the magnetosheath during most of the event, until around 22:50 UT when it crosses the magnetopause. ACE magnetic field measurements are magnified by a factor of 3 to facilitate the comparison with Cluster observations. ACE data are displayed at 16 s resolution and Cluster's at spin ( $\sim 4$  s) resolution. The green area in Figure 5 indicates when Cluster is in the magnetosphere. A magnified section of Figure 5 (fourth panel) is shown in the inset, corresponding to the interval highlighted in grey, just before Cluster enters the magnetosphere. During this period, the prevailing magnetic field components in the solar wind are  $B_x$  and  $B_y$  (Figure 5, second panel, and Figure 5, (third panel), respectively), while  $B_z$  is much weaker (Figure 5, fourth panel, and inset). Pointing initially northward,  $B_z$  turns south shortly after 21:30 UT and remains negative until the end of the event. In the magnetosheath, however, Cluster measures a steadily northward magnetic field throughout. The southward fields after 22:30 UT are magnetospheric fields. The spacecraft thus observes a

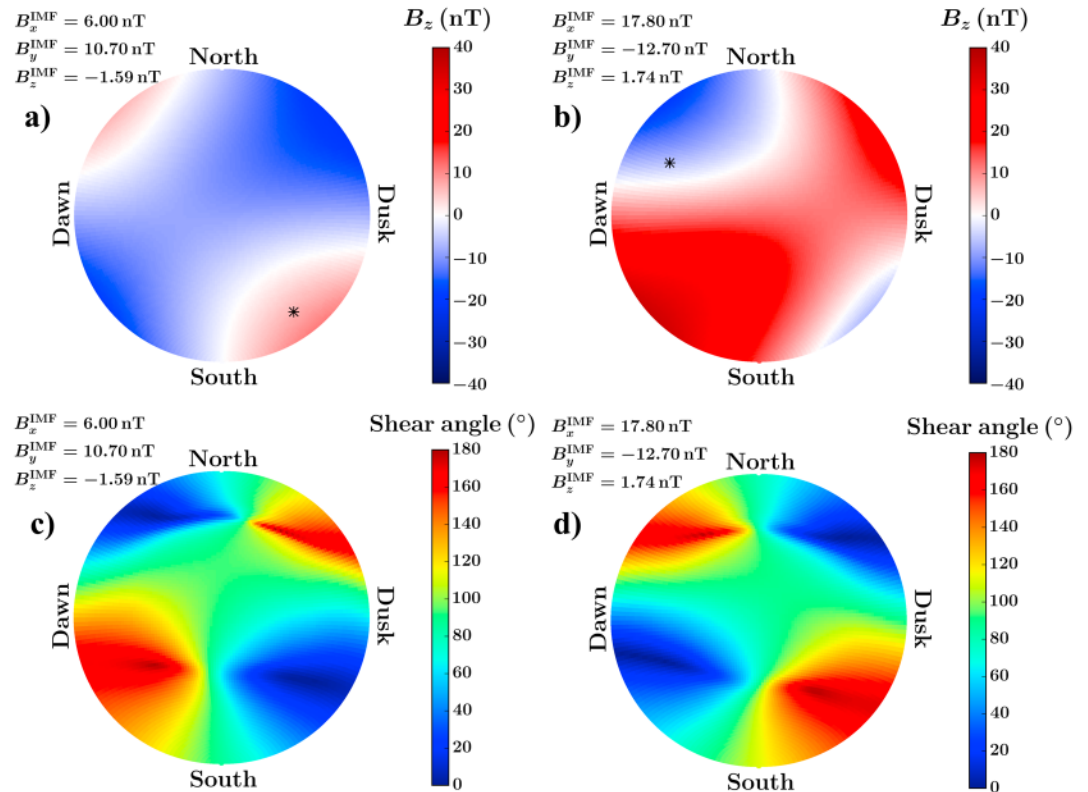


**Figure 6.** Maps of the dayside magnetopause projected onto a plane, with the subsolar point at the center and the radial distance from the center proportional to the zenithal angle.  $B_z$  component along the magnetopause during the  $B_z$  reversals observed on (a) 29 November 2006 and (b) 22 January 2012. (c and d) Shear angle along the magnetopause for the same intervals. The asterisks on Figures 4a and 4b show the position of Cluster and THEMIS A, respectively.

reversed  $B_z$  in the close vicinity of the magnetopause, which may affect the reconnection in this region provided this reversal is observed in a sizable area. One can also note that the sign of  $B_x$  measured by Cluster is opposite to the sign sampled by ACE (Figure 5, second panel), consistent with the expected orientation of the draped IMF, as Cluster is located in the duskside magnetosheath.

Using the magnetosheath model [Turc *et al.*, 2014b], we calculate the magnetosheath magnetic field along the dayside magnetopause. The solar wind parameters averaged between 21:45 UT and 22:30 UT on 29 November 2006 are employed as the input. This interval will be hereafter referred to as Event 1. Figure 6a displays the dayside magnetopause surface as seen from the Sun, color coded according to the value of the magnetic field  $B_z$  component on the outer side of the boundary. The distance from the center of the plot is proportional to the zenith angle, relative to the Sun-Earth line, ranging here from 0 to 90°, while the azimuthal direction is the angle in the plane perpendicular to the Sun-Earth line. The black star indicates Cluster’s position. As expected from the southward orientation of the upstream magnetic field,  $B_z$  is negative along most of the magnetopause (in blue). However, the model also predicts that there are two regions where  $B_z$  is positive (in red) and that Cluster is located in the largest of them. Figure 6b shows another example of a  $B_z$  reversal, observed by THEMIS A on 22 January 2012 around 14:00 UT (hereafter Event 2). The format is the same as in Figure 6a. In this second example, the upstream  $B_z$  is oriented northward. It turns south in two regions of the magnetosheath, one of them encompassing the position of THEMIS A. We find that the maximum reversed  $B_z$  (in absolute value) are 11 nT in Event 1 and –19 nT in Event 2. We calculate that 19% of the dayside magnetopause encounters a reversed  $B_z$  in Event 1 and 22% in Event 2.

We then compute the shear angle between the magnetosheath and magnetospheric magnetic fields along the magnetopause during both events. The magnetospheric magnetic field at the Shue *et al.* [1998] magnetopause is obtained from the T96 model [Tsyganenko, 1995], as done for example in Trattner *et al.* [2012, and references therein]. The results for Events 1 and 2 are displayed in Figures 6c and 6d, respectively. The shear angle maps for these two events are roughly mirror images of each other. This is due to the oppositely directed

**Table 1.** Summary of the Sources of Discrepancies Between Model and Observations

Category	Source of Discrepancies	Number of Events
(i)a	Bow shock position	4
(i)b	Magnetopause position	2
(i)c	Boundary position	3
(ii)a	Quasi-parallel configuration	9
(ii)b	Spacecraft skimming the magnetopause	8

magnetic fields in the YZ plane, with  $B_y$  and  $B_z$  respectively, positive and negative in Event 1 and vice versa in Event 2. Note that  $B_x$  is positive in both cases. For both events, we find two regions of antiparallel magnetic fields (in red), i.e., favorable to reconnection, the largest being in the Southern Hemisphere, on the dawn (Event 1) or dusk (Event 2) flank.

These maps are consistent with the reconnection pattern inferred by Němeček *et al.* [2003] from multispacecraft observations during horizontal IMF conditions (i.e., with very small  $B_z$  component), with the reconnection regions located on opposite sides of the cusps in opposite hemispheres. They are also very similar to those obtained in Trattner *et al.* [2007a, 2007b, 2012] for a southward IMF with a large  $B_y$  component (i.e., with a clock angle around  $90^\circ$  or  $270^\circ$ ). However, we remind the reader that in Event 2 the IMF  $B_z$  is actually oriented northward. Interestingly, the high shear regions are located in the same quadrants of the magnetopause as the southward turnings of the magnetic field. The  $B_z$  reversal may therefore explain why the shear angle distribution at the magnetopause in Event 2 mirrors that of Event 1. To confirm this, we calculate the shear angle along the magnetopause for the same upstream conditions but with an opposite  $B_z$  sign (not shown). For each event, we find very similar shear angle patterns for both positive and negative  $B_z$ . This suggests that the sign of  $B_z$  does not, or only marginally, affect the solar wind-magnetospheric coupling when  $B_z$  is small compared to  $B_y$ . Although we are here focusing on MC events, the maps shown in Figure 6 would be roughly the same for typical solar wind with the same IMF orientation. Our conclusions thus also hold for regular solar wind conditions.

#### 4. Discussion: Limitations of the Magnetosheath Model

We now examine the 26 sets of spacecraft observations inside the magnetosheath during a MC's passage which are not satisfactorily reproduced by the magnetosheath model. We find that they can be divided into two categories, as the discrepancies between model and observations are either due to (i) an incorrect prediction of the position of the magnetosheath boundaries (9 events) or (ii) the limitations of the ideal MHD description employed in the model (17 events). Some of the events in Category (i) are associated with extremely low ( $\sim 1$ )  $M_A$  conditions, which are at the limit of applicability of the bow shock models. Others are visibly due to an inaccurate estimate of the magnetopause position, as the model predicts the spacecraft to remain inside the magnetosphere, while its measurements show that it actually samples the magnetosheath. The remainder of the Category (i) events show an overestimation or underestimation of the magnetic field draping, which can be caused by an erroneous prediction of the position of any or both of the magnetosheath boundaries. Events in Category (ii) are either found (a) downstream of the quasi-parallel region of the bow shock or (b) when the spacecraft is skimming the magnetopause. In both regions, nonideal MHD processes can come into play, which cannot be described by the magnetosheath model. Close to the magnetopause, the magnetosheath magnetic field can be for example disturbed by reconnection, linear/nonlinear Kelvin-Helmholtz waves or turbulent flows [Coleman, 2005]. Near the quasi-parallel bow shock, the enhanced wave activity and the high level of turbulence both in the foreshock and the magnetosheath can alter the magnetic field direction [Walsh *et al.*, 2014, and references therein]. The sources of discrepancies between model and observations are summarized in Table 1.

However, it is worth noting that the model yields satisfactory results also in the quasi-parallel regime, as illustrated by the samples at  $\Theta_{Bn} < 45^\circ$  in Figure 2. We have in particular 13 events where the average  $\Theta_{Bn}$  is below  $45^\circ$  and 16 where at least one third of the samples are associated with quasi-parallel conditions. However, the discarded events in Category ((ii)a) appear to be all "strongly" quasi-parallel cases. In these events, more than 60% of the magnetosheath samples are associated with quasi-parallel conditions, and the average  $\Theta_{Bn}$  per event is generally lower than in the events for which model and observations agree well. In a few case studies,

*Turc et al.* [2014a] showed that when  $\Theta_{bn} < 30^\circ$ , the smooth rotation of the MC's magnetic field is blurred by large-amplitude fluctuations. Since such fluctuations are not included in the magnetosheath model, this may explain why no good agreement between model and observations can be obtained for very low  $\Theta_{bn}$  values. Another reason could be that magnetic coplanarity may be violated during these intervals, due to the wave activity or the nonstationarity of the bow shock [Treumann, 2009]. This may explain why we sometimes find that the model correctly predicts the overall magnetic field variation across the bow shock but not in which direction this change takes place. Note that we assume here that the  $\Theta_{bn}$  values provided by the model are reliable. The bow shock shape may depart locally from the model's predictions, due to, e.g., ripples [see, e.g., Hietala et al., 2009, and references therein], but overall, the model should provide a reasonable estimate of  $\Theta_{bn}$  in that region.

In section 3.1, we have noted that the magnetic field clock angle was only marginally modified across the bow shock. As discussed in the section 1, the deviation from "perfect draping" (i.e., no variation of the clock angle) in the magnetosheath was also investigated by *Coleman* [2005] using GEOTAIL and Interball-Tail data for 36 magnetopause crossings during non-MC conditions. This study shows that near the magnetopause, the deviation of the clock angle is below  $30^\circ$  in 70% of the cases. In the present work, however, we find that 98% of our samples are within  $30^\circ$  of the perfect draping. One of the reasons for that may be that the MC's magnetic field generally lies close to the plane perpendicular to the Sun-Earth line; i.e.,  $B_x$  is typically small [Turc et al., 2016]. It was shown by *Coleman* [2005] that such upstream conditions tend to decrease the deviation from perfect draping. Yet even when restricting our data set to low cone angle values, we still find a very small variation of the clock angle. The small  $B_x$  component inside MCs is therefore not sufficient to explain the discrepancies between our results and the findings of *Coleman* [2005]. We note, however, that in 8 of the 9 discarded events when the bow shock is in quasi-parallel configuration, a large ( $\geq 30^\circ$ ) modification of the clock angle is observed. This implies that the largest deviations from perfect draping are actually discarded from our data set. This also suggests that the crossing of the quasi-parallel bow shock can result in a significant variation of the clock angle. In those cases, the magnetosheath model fails to reproduce such large changes of the clock angle but generally gives a reasonable estimate of the  $\psi$  angle. In other words, the overall variation is correctly predicted but not in which direction the magnetic field vector rotates. Therefore, the discrepancies between model and observations might be caused by magnetic coplanarity not being satisfied across the bow shock.

Interestingly, in three of the events with a large variation of the clock angle, long-duration (1 to 3 h) reversals of the  $B_z$  component are observed. Two events are similar to those discussed in section 3.2, with  $\theta_{sw} \sim 90^\circ$ . In the other, however, the upstream magnetic field direction lies up to about  $30^\circ$  from the equatorial plane ( $\theta_{sw} \sim 120^\circ$ ), while most of the blue samples in Figure 4c were found within  $10^\circ$  of this plane. The large variation of the clock angle thus allows  $B_z$  to reverse in that case. The magnetosheath  $B_z$  is also higher, up to 20 nT, than the other reversed  $B_z$  (see the blue data points in Figure 4b). This  $B_z$  reversal is observed downstream of a strongly parallel shock ( $\Theta_{bn} \sim 20\text{--}30^\circ$ ). This suggests that our results based on the magnetosheath model provide a lower limit of the extent and occurrence rate of the  $B_z$  reversal but that there may be more significant changes in  $B_z$  when the shock is strongly parallel.

## 5. Summary and Conclusions

Using 82 MCs with simultaneous observations in the solar wind and the magnetosheath, we have carried out a statistical study of the modification of their magnetic structure across the bow shock. Our main results are the following:

1. We have confirmed statistically that the angle measured between the solar wind and magnetosheath magnetic field direction is controlled by two processes: the bow shock crossing and the draping of the field lines. Far enough from the magnetopause, where the draping effects are not predominant, that is, in the first 30% of the magnetosheath, we empirically find that the relationship between the local change in the magnetic field orientation and the angle  $\Theta_{bn}$  encountered at the bow shock's crossing is approximately linear for  $\Theta_{bn} > 30^\circ$ . This linear relationship is in good agreement with MHD predictions for this range of  $\Theta_{bn}$  (see Figure 2).
2. The variation of the magnetic field direction takes place essentially through a modification of its cone angle. Large rotations of the magnetic field clock angle are observed only in a few cases. They all appear to be associated with strongly quasi-parallel shock configurations. However, those events are

- generally not satisfactorily reproduced by the magnetosheath model and are therefore excluded from our statistical analysis.
3. The sign of the solar wind  $B_z$  is not always preserved in the magnetosheath. We find evidence of opposite  $B_z$  signs on either sides of the bow shock. In particular, during three events, the  $B_z$  reversal lasts half an hour or more. We find that such reversals occur when the upstream magnetic field lies close to the equatorial plane.
  4. Using a magnetosheath model, we estimate the extent of the region where  $B_z$  reverses. We find that it affects a significant ( $\sim 20\%$ ) part of the magnetopause. Maps of the shear angle along the magnetopause reveal that the regions favorable to reconnection follow the patterns expected for  $B_y$ -dominated conditions, independently of the sign of  $B_z$  in the upstream medium. This suggests that if the predominant IMF component is  $B_y$ , positive and negative  $B_z$  could be equally geoeffective.
  5. The comparison of the results of the *Turc et al.* [2014b] magnetosheath model with spacecraft observations for 129 events shows that this model reproduces well the magnetic field direction inside the magnetosheath in most cases (80%). This implies that MHD is in general sufficient to capture the transition through the bow shock and the magnetosheath during MCs. This may be due to the bow shock being mostly quasi-perpendicular in MC conditions [*Turc et al.*, 2016].
  6. We also establish the limits of applicability of the *Turc et al.* [2014b] magnetosheath model. The model's outputs are mostly reliable (i.e., the differences between model and observations are within  $10^\circ$  for most of the samples, and the overall temporal variations are correctly reproduced by the model) when the shock is not strongly parallel ( $\Theta_{bn} \geq 20^\circ$ ), the spacecraft is not skimming the magnetopause and the Alfvén Mach number is not approaching 1. This is consistent with the ideal MHD description on which the model is based. Within its limits of applicability, i.e. excluding the nine strongly parallel events ((ii)a), the eight events in the vicinity of the magnetopause ((ii)b) and the four events with dramatically low  $M_A$  ((i)a), the model provides reliable predictions of the magnetosheath magnetic field direction for 95% of the events (103/108).

In some instances, the position of the magnetosheath boundaries is not properly described by the models employed here [*Shue et al.*, 1998; *Jeřáb et al.*, 2005; *Měrka et al.*, 2005], thus leading to incorrect results of the magnetosheath model. The performances of the *Shue et al.* [1998] magnetopause model have been investigated by *Case and Wild* [2013], who showed that this model tends to overestimate the magnetopause position. The authors suggest that this may be due to the data set on which the model was build. As regards the bow shock models, the sources of the discrepancies are not clear, except for the very low  $M_A$  conditions, and identifying them lies beyond the scope of this paper. Improved bow shock and magnetopause models could solve this issue and would therefore allow for more events to be properly modeled. Overall, the *Turc et al.* [2014b] magnetosheath model performs well for the majority of events.

Though the present study shows evidence of  $B_z$  changing sign from the solar wind to the magnetosheath, it does not, however, allow us to estimate reliably the occurrence rate of the  $B_z$  reversals, for the following reasons. (1) The  $B_z$  reversals only take place in a limited (though significant,  $\sim 20\%$  in the examples given here) part of the magnetosheath for a given IMF configuration. Furthermore, most spacecraft orbit close to the equatorial plane, while the  $B_z$  reversals generally occur at higher latitudes (see Figures 6a and 6b). The reversal of  $B_z$  may therefore be missed in a number of events due to the limited coverage provided by spacecraft observations. (2) Our selection criteria for our magnetosheath samples require a good agreement between the modeled and observed magnetic fields, but  $B_z$  reversals can also occur when ideal MHD is not satisfied. In particular, significant  $B_z$  reversals are observed when the shock is strongly parallel, but the magnetosheath model is not valid in such conditions, as discussed in section 4. These events are thus not taken into account in the results shown in section 3.2. We also note that the probability of observation of a change of the  $B_z$  sign is lower in our data set than in the results of *Šafránková et al.* [2009]. This may stem from the higher magnetic field strength during MCs, since *Šafránková et al.* [2009] showed that this probability decreases with increasing magnetic field magnitude; (2) can also contribute to this lower probability. Furthermore, we only retained those samples where  $B_z$  and  $B_z \pm \sigma$  have identical signs, to ensure that the  $B_z$  reversal is significant. No such criterion was applied to the *Šafránková et al.* [2009] data set. Finally, although the  $B_z$  reversals are observed only in a limited number of events, their spatial and temporal extent suggests that they may affect the interaction of these MCs with the magnetosphere.

To conclude, there is clear evidence that the magnetic field direction inside MCs can be significantly modified downstream of the Earth's bow shock and that the largest changes are associated with the quasi-parallel shock configuration. This should also hold for regular solar wind conditions, but it is more apparent during MCs as the upstream magnetic field direction varies but slowly over extended intervals. These changes of the

magnetic field orientation may have strong implications in terms of reconnection at the magnetopause. As a consequence, the effects of MCs on the magnetosphere may sometimes differ from what could be expected from the sole analysis of their properties near  $L_1$ . We also stress the importance of not only taking into account the  $B_z$  component when assessing the possible geoeffectivity of a MC. This is exemplified by the fact that northward and southward  $B_z$  both lead to similar shear angle patterns at the magnetopause when  $B_y$  is predominant. The modification of  $B_z$  inside the magnetosheath when  $B_y$  is predominant may also affect the duration of the geoeffective part of the MC, in particular during the so-called bipolar MCs [Mulligan *et al.*, 1998]. In the central part of such MCs,  $B_y$  is predominant while  $B_z$  turns progressively either from positive to negative or from negative to positive. Only the rear part of the former or the front part of the latter is expected to be geoeffective. However, if  $B_z$  changes sign at different times in the magnetosheath and in the solar wind, this may affect the onset or end time of geomagnetic activity. Taking this into account may contribute to improve space weather forecasting. Further work is still required to quantify the influence of the bow shock and the magnetosheath on the geoeffectivity of MCs and thus refine our understanding of the interaction of MCs with the Earth's environment.

#### Acknowledgments

The authors are thankful to the PIs who have made available the various data sets used in this study. We thank the Coordinated Data Analysis Web (CDAWeb) service (<http://cdaweb.gsfc.nasa.gov/spphys/>) for providing ACE, Wind, OMNI, GEOTAIL, THEMIS, and Interball data and the Cluster Science Archive (CSA) [Laakso *et al.*, 2010] for providing Cluster and Double-Star data. L.T. is supported by an ESA Research Fellowship in Space Science. A.P. Dimmock was supported by the Academy of Finland grant 288472. All data used in this paper are publicly available on the CDAWeb and the CSA.

#### References

- Acuña, M. H., K. W. Ogilvie, D. N. Baker, S. A. Curtis, D. H. Fairfield, and W. H. Mish (1995), The global geospace science program and its investigations, *Space Sci. Rev.*, *71*, 5–21, doi:10.1007/BF00751323.
- Angelopoulos, V. (2008), The THEMIS mission, *Space Sci. Rev.*, *141*, 5–34, doi:10.1007/s11214-008-9336-1.
- Auster, H. U., et al. (2008), The THEMIS fluxgate magnetometer, *Space Sci. Rev.*, *141*, 235–264, doi:10.1007/s11214-008-9365-9.
- Balogh, A., et al. (1997), The cluster magnetic field investigation, *Space Sci. Rev.*, *79*, 65–91, doi:10.1023/A:1004970907748.
- Borovsky, J. E. (2013), Physical improvements to the solar wind reconnection control function for the Earth's magnetosphere, *J. Geophys. Res. Space Physics*, *118*, 2113–2121, doi:10.1002/jgra.50110.
- Burlaga, L. F., E. Sittler, F. Mariani, and R. Schwenn (1981), Magnetic loop behind an interplanetary shock—Voyager, Helios, and IMP 8 observations, *J. Geophys. Res.*, *86*, 6673–6684, doi:10.1029/JA086iA08p06673.
- Carr, C., et al. (2005), The Double Star magnetic field investigation: Instrument design, performance and highlights of the first year's observations, *Ann. Geophys.*, *23*, 2713–2732, doi:10.5194/angeo-23-2713-2005.
- Case, N. A., and J. A. Wild (2013), The location of the Earth's magnetopause: A comparison of modeled position and in situ Cluster data, *J. Geophys. Res. Space Physics*, *118*, 6127–6135, doi:10.1002/jgra.50572.
- Coleman, I. J. (2005), A multi-spacecraft survey of magnetic field line draping in the dayside magnetosheath, *Ann. Geophys.*, *23*, 885–900, doi:10.5194/angeo-23-885-2005.
- Dimmock, A. P., and K. Nykyri (2013), The statistical mapping of magnetosheath plasma properties based on THEMIS measurements in the magnetosheath interplanetary medium reference frame, *J. Geophys. Res. Space Physics*, *118*, 4963–4976, doi:10.1002/jgra.50465.
- Dimmock, A. P., K. Nykyri, H. Karimabadi, A. Osmane, and T. I. Pulkkinen (2015), A statistical study into the spatial distribution and dawn-dusk asymmetry of dayside magnetosheath ion temperatures as a function of upstream solar wind conditions, *J. Geophys. Res. Space Physics*, *120*, 2767–2782, doi:10.1002/2014JA020734.
- Dimmock, A. P., T. I. Pulkkinen, A. Osmane, and K. Nykyri (2016), The dawn-dusk asymmetry of ion density in the dayside magnetosheath and its annual variability measured by THEMIS, *Ann. Geophys.*, *34*, 511–528, doi:10.5194/angeo-34-511-2016.
- Dungey, J. W. (1961), Interplanetary magnetic field and the auroral zones, *Phys. Rev. Lett.*, *6*, 47–48, doi:10.1103/PhysRevLett.6.47.
- Eastwood, J. P., A. Balogh, M. W. Dunlop, and C. W. Smith (2002), Cluster observations of the heliospheric current sheet and an associated magnetic flux rope and comparisons with ACE, *J. Geophys. Res.*, *107*(A11), 1365, doi:10.1029/2001JA009158.
- Echer, E., W. D. Gonzalez, and B. T. Tsurutani (2008), Interplanetary conditions leading to superintense geomagnetic storms ( $D_{st} \leq -250$  nT) during solar cycle 23, *Geophys. Res. Lett.*, *35*, L06S03, doi:10.1029/2007GL031755.
- Erkaev, N. V., C. J. Farrugia, A. V. Mezentsev, R. B. Torbert, and H. K. Biernat (2012), Accelerated magnetosheath flows caused by IMF draping: Dependence on latitude, *Geophys. Res. Lett.*, *39*, L01103, doi:10.1029/2011GL050209.
- Escoubet, C. P., M. Fehringer, and M. Goldstein (2001), Introduction The Cluster mission, *Ann. Geophys.*, *19*, 1197–1200, doi:10.5194/angeo-19-1197-2001.
- Farris, M. H., and C. T. Russell (1994), Determining the standoff distance of the bow shock: Mach number dependence and use of models, *J. Geophys. Res.*, *99*, 17,681–17,689, doi:10.1029/94JA01020.
- Farrugia, C. J., N. V. Erkaev, V. K. Jordanova, N. Lugaz, P. E. Sandholt, S. Mühlbacher, and R. B. Torbert (2013), Features of the interaction of interplanetary coronal mass ejections/magnetic clouds with the Earth's magnetosphere, *J. Atmos. Sol. Terr. Phys.*, *99*, 14–26, doi:10.1016/j.jastp.2012.11.014.
- Galeev, A. A., Y. I. Galperin, and L. M. Zelenyi (1996), The INTERBALL project to study solar-terrestrial physics, *Cosmic Res.*, *34*, 313.
- Génot, V., L. Broussillou, E. Budnik, P. Hellinger, P. M. Trávníček, E. Lucek, and I. Dandouras (2011), Timing mirror structures observed by Cluster with a magnetosheath flow model, *Ann. Geophys.*, *29*, 1849–1860, doi:10.5194/angeo-29-1849-2011.
- Gopalswamy, N., S. Akiyama, S. Yashiro, G. Michalek, and R. P. Lepping (2008), Solar sources and geospace consequences of interplanetary magnetic clouds observed during solar cycle 23, *J. Atmos. Sol. Terr. Phys.*, *70*, 245–253, doi:10.1016/j.jastp.2007.08.070.
- Hasegawa, H., M. Fujimoto, T.-D. Phan, H. Rème, A. Balogh, M. W. Dunlop, C. Hashimoto, and R. TanDokoro (2004), Transport of solar wind into Earth's magnetosphere through rolled-up Kelvin-Helmholtz vortices, *Nature*, *430*, 755–758, doi:10.1038/nature02799.
- Hidalgo, M. A., J. J. Blanco, F. J. Alvarez, and T. Nieves-Chinchilla (2011), On the relationship between magnetic clouds and the great geomagnetic storms associated with the period 1995–2006, *J. Atmos. Sol. Terr. Phys.*, *73*, 1372–1379, doi:10.1016/j.jastp.2011.02.017.
- Hietala, H., T. V. Laitinen, K. Andréová, R. Vainio, A. Vaivads, M. Palmroth, T. I. Pulkkinen, H. E. J. Koskinen, E. A. Lucek, and H. Rème (2009), Supermagnetosonic jets behind a collisionless quasiparallel shock, *Phys. Rev. Lett.*, *103*(24), 245001, doi:10.1103/PhysRevLett.103.245001.
- Huttunen, K. E. J., R. Schwenn, V. Bothmer, and H. E. J. Koskinen (2005), Properties and geoeffectiveness of magnetic clouds in the rising, maximum and early declining phases of solar cycle 23, *Ann. Geophys.*, *23*(2), 625–641, doi:10.5194/angeo-23-625-2005.
- Jeřáb, M., Z. Němeček, J. Šafránková, K. Jelínek, and J. Měrka (2005), Improved bow shock model with dependence on the IMF strength, *Planet. Space. Sci.*, *53*, 85–93, doi:10.1016/j.pss.2004.09.032.

- Ji, E.-Y., Y.-J. Moon, K.-H. Kim, and D.-H. Lee (2010), Statistical comparison of interplanetary conditions causing intense geomagnetic storms ( $Dst \leq -100$  nT), *J. Geophys. Res.*, *115*, A10232, doi:10.1029/2009JA015112.
- Klimov, S., et al. (1997), ASPI experiment: Measurements of fields and waves on board the INTERBALL-1 spacecraft, *Ann. Geophys.*, *15*, 514–527, doi:10.1007/s00585-997-0514-3.
- Kobel, E., and E. O. Flückiger (1994), A model of the steady state magnetic field in the magnetosheath, *J. Geophys. Res.*, *99*, 23,617–23,622, doi:10.1029/94JA01778.
- Kokubun, S., T. Yamamoto, M. H. Acuña, K. Hayashi, K. Shiokawa, and H. Kawano (1994), The GEOTAIL magnetic field experiment, *J. Geomagn. Geoelectr.*, *46*, 7–21.
- Laakso, H., C. Perry, S. McCaffrey, D. Herment, A. J. Allen, C. C. Harvey, C. P. Escoubet, C. Gruenberger, M. G. G. Taylor, and R. Turner (2010), Cluster active archive: Overview, *Astrophys. Space Sci. Proc.*, *11*, 3–37, doi:10.1007/978-90-481-3499-1\_1.
- Landau, L. Q., and E. M. Lifshitz (1959), *Fluid Mechanics*, Pergamon, New York.
- Lavraud, B., and J. E. Borovsky (2008), Altered solar wind-magnetosphere interaction at low Mach numbers: Coronal mass ejections, *J. Geophys. Res.*, *113*, A00B08, doi:10.1029/2008JA013192.
- Lavraud, B., J. E. Borovsky, A. J. Ridley, E. W. Pogue, M. F. Thomsen, H. Rème, A. N. Fazakerley, and E. A. Lucek (2007), Strong bulk plasma acceleration in Earth's magnetosheath: A magnetic slingshot effect?, *Geophys. Res. Lett.*, *34*, L14102, doi:10.1029/2007GL030024.
- Lavraud, B., et al. (2013), Asymmetry of magnetosheath flows and magnetopause shape during low Alfvén Mach number solar wind, *J. Geophys. Res. Space Physics*, *118*, 1089–1100, doi:10.1002/jgra.50145.
- Lepping, R. P., et al. (1995), The wind magnetic field investigation, *Space Sci. Rev.*, *71*, 207–229, doi:10.1007/BF00751330.
- Liu, Z. X., C. P. Escoubet, Z. Pu, H. Laakso, J. K. Shi, C. Shen, and M. Hapgood (2005), The Double Star mission, *Ann. Geophys.*, *23*, 2707–2712, doi:10.5194/angeo-23-2707-2005.
- Longmore, M., S. J. Schwartz, and E. A. Lucek (2006), Rotation of the magnetic field in Earth's magnetosheath by bulk magnetosheath plasma flow, *Ann. Geophys.*, *24*, 339–354, doi:10.5194/angeo-24-339-2006.
- Lopez, R. E., M. Wiltberger, S. Hernandez, and J. G. Lyon (2004), Solar wind density control of energy transfer to the magnetosphere, *Geophys. Res. Lett.*, *31*, L08804, doi:10.1029/2003GL018780.
- Lopez, R. E., R. Bruntz, E. J. Mitchell, M. Wiltberger, J. G. Lyon, and V. G. Merkin (2010), Role of magnetosheath force balance in regulating the dayside reconnection potential, *J. Geophys. Res.*, *115*, A12216, doi:10.1029/2009JA014597.
- Lopez, R. E., V. G. Merkin, and J. G. Lyon (2011), The role of the bow shock in solar wind-magnetosphere coupling, *Ann. Geophys.*, *29*, 1129–1135, doi:10.5194/angeo-29-1129-2011.
- McComas, D. J., S. J. Bame, P. Barker, W. C. Feldman, J. L. Phillips, P. Riley, and J. W. Griffee (1998), Solar Wind Electron Proton Alpha Monitor (SWEPAM) for the advanced composition explorer, *Space Sci. Rev.*, *86*, 563–612, doi:10.1023/A:1005040232597.
- Mulligan, T., C. T. Russell, and J. G. Luhmann (1998), Solar cycle evolution of the structure of magnetic clouds in the inner heliosphere, *Geophys. Res. Lett.*, *25*, 2959–2962, doi:10.1029/98GL01302.
- Mérka, J., A. Szabo, J. A. Slavin, and M. Peredo (2005), Three-dimensional position and shape of the bow shock and their variation with upstream Mach numbers and interplanetary magnetic field orientation, *J. Geophys. Res.*, *110*, A04202, doi:10.1029/2004JA010944.
- Myllys, M., E. K. J. Kilpua, B. Lavraud, and T. I. Pulkkinen (2016), Solar wind-magnetosphere coupling efficiency during ejecta and sheath-driven geomagnetic storms, *J. Geophys. Res. Space Physics*, *121*, 4378–4396, doi:10.1002/2016JA022407.
- Nishida, A. (1994), The GEOTAIL mission, *Geophys. Res. Lett.*, *21*, 2871–2873, doi:10.1029/94GL01223.
- Nozdrachev, M., V. Styazhkin, A. Zarutsky, S. Klimov, and S. E. Savin (1995), Magnetic field measurements onboard the Interball Tail spacecraft: The FM-3I instrument, in *INTERBALL Mission and Payload*, edited by RKA-IKI-CNES, pp. 228–229, CNES, France.
- Němeček, Z., et al. (2003), Structure of the outer cusp and sources of the cusp precipitation during intervals of a horizontal IMF, *J. Geophys. Res.*, *108*(A12), 1420, doi:10.1029/2003JA009916.
- Němeček, Z., J. Šafránková, O. Kruparova, L. Přech, K. Jelínek, V. Dušík, J. Šimůnek, K. Grygorov, and J.-H. Shue (2015), Analysis of temperature versus density plots and their relation to the LLBL formation under southward and northward IMF orientations, *J. Geophys. Res. Space Physics*, *120*, 3475–3488, doi:10.1002/2014JA020308.
- Nykyri, K. (2013), Impact of MHD shock physics on magnetosheath asymmetry and Kelvin-Helmholtz instability, *J. Geophys. Res. Space Physics*, *118*, 5068–5081, doi:10.1002/jgra.50499.
- Ogilvie, K. W., et al. (1995), SWE, a comprehensive plasma instrument for the wind spacecraft, *Space Sci. Rev.*, *71*, 55–77, doi:10.1007/BF00751326.
- Pulkkinen, T. I., A. P. Dimmock, A. Lakka, A. Osmane, E. K. J. Kilpua, M. Myllys, E. I. Tanskanen, and A. Viljanen (2016), Magnetosheath control of solar wind-magnetosphere coupling efficiency, *J. Geophys. Res. Space Physics*, *121*, 8728–8739, doi:10.1002/2016JA023011.
- Rosenqvist, L., A. Kullen, and S. Buchert (2007), An unusual giant spiral arc in the polar cap region during the northward phase of a coronal mass ejection, *Ann. Geophys.*, *25*, 507–517, doi:10.5194/angeo-25-507-2007.
- Šafránková, J., M. Hayosh, O. Gutynska, Z. Němeček, and L. Přech (2009), Reliability of prediction of the magnetosheath  $B_z$  component from interplanetary magnetic field observations, *J. Geophys. Res.*, *114*, A12213, doi:10.1029/2009JA014552.
- Shue, J.-H., et al. (1998), Magnetopause location under extreme solar wind conditions, *J. Geophys. Res.*, *103*, 17,691–17,700, doi:10.1029/98JA01103.
- Smith, C. W., J. L'Heureux, N. F. Ness, M. H. Acuña, L. F. Burlaga, and J. Scheifele (1998), The ACE magnetic fields experiment, *Space Sci. Rev.*, *86*, 613–632, doi:10.1023/A:1005092216668.
- Soucek, J., and C. P. Escoubet (2012), Predictive model of magnetosheath plasma flow and its validation against Cluster and THEMIS data, *Ann. Geophys.*, *30*, 973–982, doi:10.5194/angeo-30-973-2012.
- Stone, E. C., A. M. Frandsen, R. A. Mewaldt, E. R. Christian, D. Margolies, J. F. Ormes, and F. Snow (1998), The Advanced Composition Explorer, *Space Sci. Rev.*, *86*, 1–22, doi:10.1023/A:1005082526237.
- Taylor, M. G. G. T., et al. (2012), Spatial distribution of rolled up Kelvin-Helmholtz vortices at Earth's dayside and flank magnetopause, *Ann. Geophys.*, *30*, 1025–1035, doi:10.5194/angeo-30-1025-2012.
- Trattner, K. J., J. S. Mulcock, S. M. Petrinec, and S. A. Fuselier (2007a), Location of the reconnection line at the magnetopause during southward IMF conditions, *Geophys. Res. Lett.*, *34*, L03108, doi:10.1029/2006GL028397.
- Trattner, K. J., J. S. Mulcock, S. M. Petrinec, and S. A. Fuselier (2007b), Probing the boundary between antiparallel and component reconnection during southward interplanetary magnetic field conditions, *J. Geophys. Res.*, *112*, A08210, doi:10.1029/2007JA012270.
- Trattner, K. J., S. M. Petrinec, S. A. Fuselier, and T. D. Phan (2012), The location of reconnection at the magnetopause: Testing the maximum magnetic shear model with THEMIS observations, *J. Geophys. Res.*, *117*, A01201, doi:10.1029/2011JA016959.
- Treumann, R. A. (2009), Fundamentals of collisionless shocks for astrophysical application: 1. Non-relativistic shocks, *Astron. Astrophys. Rev.*, *17*, 409–535, doi:10.1007/s00159-009-0024-2.

- Tsyganenko, N. A. (1995), Modeling the Earth's magnetospheric magnetic field confined within a realistic magnetopause, *J. Geophys. Res.*, *100*, 5599–5612, doi:10.1029/94JA03193.
- Turc, L., D. Fontaine, P. Savoini, H. Hietala, and E. K. J. Kilpua (2013), A comparison of bow shock models with Cluster observations during low Alfvén Mach number magnetic clouds, *Ann. Geophys.*, *31*, 1011–1019, doi:10.5194/angeo-31-1011-2013.
- Turc, L., D. Fontaine, P. Savoini, and E. K. J. Kilpua (2014a), Magnetic clouds' structure in the magnetosheath as observed by Cluster and Geotail: Four case studies, *Ann. Geophys.*, *32*, 1247–1261, doi:10.5194/angeo-32-1247-2014.
- Turc, L., D. Fontaine, P. Savoini, and E. K. J. Kilpua (2014b), A model of the magnetosheath magnetic field during magnetic clouds, *Ann. Geophys.*, *32*, 157–173, doi:10.5194/angeo-32-157-2014.
- Turc, L., D. Fontaine, P. Savoini, and R. Modolo (2015), 3D hybrid simulations of the interaction of a magnetic cloud with a bow shock, *J. Geophys. Res. Space Physics*, *120*, 6133–6151, doi:10.1002/2015JA021318.
- Turc, L., C. P. Escoubet, D. Fontaine, E. K. J. Kilpua, and S. Enestam (2016), Cone angle control of the interaction of magnetic clouds with the Earth's bow shock, *Geophys. Res. Lett.*, *43*, 4781–4789, doi:10.1002/2016GL068818.
- Walsh, A. P., S. Haaland, C. Forsyth, A. M. Keesee, J. Kissinger, K. Li, A. Runov, J. Soucek, B. M. Walsh, S. Wing, and M. G. T. Taylor (2014), Dawn-dusk asymmetries in the coupled solar wind-magnetosphere-ionosphere system: A review, *Ann. Geophys.*, *32*(7), 705–737, doi:10.5194/angeo-32-705-2014.
- Walsh, B. M., D. G. Sibeck, Y. Wang, and D. H. Fairfield (2012), Dawn-dusk asymmetries in the Earth's magnetosheath, *J. Geophys. Res.*, *117*, A12211, doi:10.1029/2012JA018240.
- Yermolaev, Y. I., N. S. Nikolaeva, I. G. Lodkina, and M. Y. Yermolaev (2012), Geoeffectiveness and efficiency of CIR, sheath, and ICME in generation of magnetic storms, *J. Geophys. Res.*, *117*, A00L07, doi:10.1029/2011JA017139.